PHYSICAL REVIEW B **87**, 060507(R) (2013)

Transport and thermodynamic properties of $(Ca_{1-x}La_x)_{10}(Pt_3As_8)(Fe_2As_2)_5$ superconductors

N. Ni,[1,2,3,4] W. E. Straszheim,[5] D. J. Williams,[1] M. A. Tanatar,[5] R. Prozorov,[5] E. D. Bauer,[1] F. Ronning,[1] J. D. Thompson,[1] and R. J. Cava[2]

[1]*Los Alamos National Laboratory, Los Alamos, New Mexico 87544, USA*
[2]*Department of Chemistry, Princeton University, Princeton, New Jersey 08544, USA*
[3]*Department of Physics and Astronomy, University of California, Los Angeles, California 90095, USA*
[4]*California Nanosystems Institute, University of California, Los Angeles, California 90095, USA*
[5]*Ames Laboratory and Department of Physics and Astronomy, Iowa State University, Ames, Iowa 50011, USA*

(Received 17 December 2012; revised manuscript received 4 February 2013; published 22 February 2013)

Single crystals of $(Ca_{1-x}La_x)_{10}(Pt_3As_8)(Fe_2As_2)_5$ ($x = 0$–0.182) superconductors have been grown and characterized by x-ray, microprobe, transport, and thermodynamic measurements. Features in the magnetic susceptibility, specific heat, and two kinks in the derivative of the electrical resistivity around 100 K in the $x = 0$ compound support the existence of decoupled structural and magnetic phase transitions. With La doping, the structural/magnetic phase transitions are suppressed and a half dome of superconductivity with a maximal T_c around 26 K is observed in the temperature-concentration phase diagram.

DOI: 10.1103/PhysRevB.87.060507 PACS number(s): 74.70.Xa, 74.25.Dw, 74.25.Bt, 74.25.F–

The report of superconductivity at 26 K in $LaFeAsO_{0.9}F_{0.1}$ (Ref. 1) has led to the discovery of several families of high T_c iron arsenide superconductors, including the so-called 1111, 122, 111, and 42 622 families.[2–4] The intense study of these families has enriched our understanding of the interplay among structure, magnetism, and superconductivity. Recently a new iron-arsenide compound, $Ca_{10}(Pt_3As_8)(Fe_2As_2)_5$ (the so-called 10-3-8 compound), has been characterized.[5–7] This compound crystallizes in a triclinic structure with space group P-1 and has -Ca-(Pt_3As_8)-Ca-(Fe_2As_2)- layer stacking, as shown in the left inset of Fig. 1. The FeAs layer is made of edge-sharing $FeAs_4$ tetrahedra, the key structural element in all the Fe-pnictide superconductors. A structural phase transition around 100 K has been revealed in this compound using polarized light imaging.[8] Although the susceptibility drop observed to accompany the long range antiferromagnetic ordering in the 1111 and 122 families has yet to be reported for the 10-3-8 parent compound,[5,9] recent NMR measurements show that this compound orders antiferromagnetically (AFM) below ∼100 K.[10] With Pt substitution on the Fe sites, superconductivity up to 12 K has been realized.[5,9] In the 1111 and 122 families, doping on the intermediary layer results in a higher T_c than doping on the FeAs layers, and thus higher T_c may be expected for intermediary layer doping in the 10-3-8 compound as well. Indeed, 20% La doping on the Ca sites in this compound was found to show a T_c of 30 K.[11] In this Rapid Communication, we report the systematic characterization of $(Ca_{1-x}La_x)_{10}(Pt_3As_8)(Fe_2As_2)_5$ single crystals via x-ray diffraction, microprobe, transport, and thermodynamic measurements. Due to the improved quality of the single crystals, we are able to observe a resistivity jump, a susceptibility drop, and a specific heat jump in the parent 10-3-8 compound, supporting the existence of both structural and magnetic phase transitions. A T-x phase diagram for $(Ca_{1-x}La_x)_{10}(Pt_3As_8)(Fe_2As_2)_5$ is presented.

Platelike millimeter-sized single crystals were successfully grown from a CaAs-rich flux.[5] CaAs, FeAs, and LaAs precursors were made using the solid state reaction method. These precursors and Pt powder were mixed thoroughly according to the nominal ratios listed in Table I; the total batch size was approximately 0.5 g. The mixture was pressed into a pellet, put in an Al_2O_3 crucible, and sealed into a quartz tube under vacuum. The resulting ampules were heated up to 1150 °C, held for 96 h, slowly cooled down to 885 °C, and then quenched. After rinsing off the flux using distilled water, single crystals were obtained. These single crystals show a layered growth habit and are easily exfoliated and bent. In each batch, small crystals, with thickness less than 0.03 mm, were employed in the transport measurements. The La concentration x was obtained via wavelength dispersive spectroscopy (WDS) using the electron probe microanalyzer of a JEOL JXA-8200 electron microprobe. WDS was performed on the measured transport samples to provide a reliable determination of the electronic phase diagram as a function of composition. The results of the WDS measurements are summarized in Table I. These measurements directly indicate that La has been successfully doped on the Ca sites, while the Pt substitution on the FeAs layer is well controlled: It is 0 for the $x = 0$ compound; 0.007 for the $x = 0.021$, 0.043, 0.065, and 0.145 compounds; and 0.02 for the $x = 0.093$ and 0.182 compounds. In this Rapid Communication, x refers to the WDS value. Transport and specific heat measurements were performed in a Quantum Design (QD) physical properties measurement system. Magnetic properties were measured in a QD magnetic properties measurement system. To easily compare the physical properties of these superconductors with other iron arsenide superconductors, the units of molar susceptibility, magnetization, and heat capacity presented are normalized to per mole Fe_2.

X-ray diffraction was performed on a Scintag X_1 Advances Diffraction System employing Cu $K\alpha$ ($\lambda = 1.5406$ Å) radiation. No FeAs, $PtAs_2$, or other impurities were observed in any x-ray pattern. Figure 1 shows the $(00L)$ diffraction pattern of $(Ca_{1-x}La_x)_{10}(Pt_3As_8)(Fe_2As_2)_5$ ($x = 0,0.182$). A peak shift between these two samples is observed. By refining the $(00L)$ diffraction patterns via the UNITCELL software[12] the interlayer distances of the FeAs layers were obtained. The right inset of Fig. 1 shows the evolution of the interlayer FeAs distance with x. This distance increases monotonically with La doping

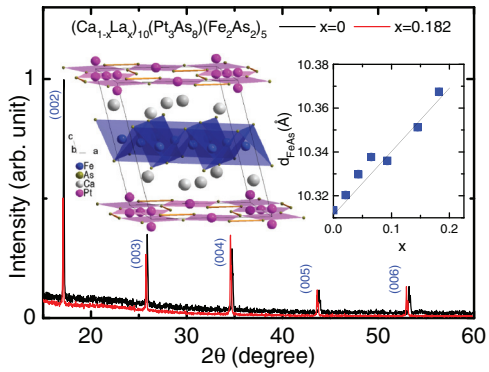

FIG. 1. (Color online) The (00l) diffraction pattern of $(Ca_{1-x}La_x)_{10}(Pt_3As_8)(Fe_2As_2)_5$ ($x = 0$,0.182). Left inset: The crystal structure of $Ca_{10}(Pt_3As_8)(Fe_2As_2)_5$. Right inset: The interlayer FeAs distance vs doping level x.

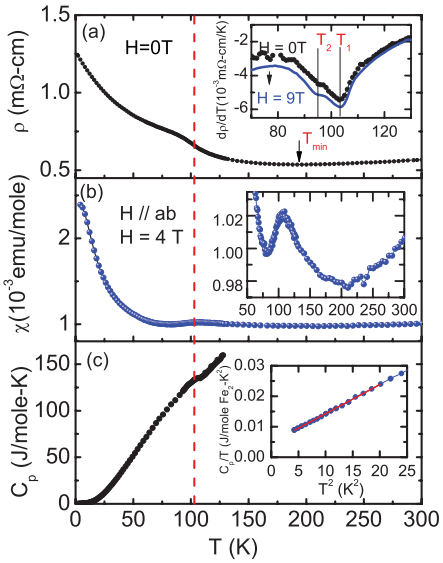

FIG. 2. (Color online) The physical properties of $Ca_{10}(Pt_3As_8)(Fe_2As_2)_5$. (a) Electrical resistivity $\rho(T)$ taken at $H = 0$ T. Inset: $d\rho/dT$ vs T taken at 0 and 9 T; $T_1 = 103$ K and $T_2 = 95$ K. (b) $\chi(T)$ taken at 4 T with $H \parallel ab$. Inset: The $\chi(T)$ from 50 to 300 K. (c) C_p vs T. Inset: C_p/T vs. T^2. The units of molar susceptibility and heat capacity presented are normalized to per mole Fe_2.

from 10.313(2) Å in the parent compound to 10.368(2) Å in the $x = 0.182$ compound, providing further evidence that La is incorporated into the structure.

The physical properties of the parent compound are summarized in Fig. 2. Figure 2(a) shows the temperature dependence of the resistivity. The resistivity is 0.57 mΩ cm at 300 K, which is almost twice as that of $BaFe_2As_2$.[13,14] $\rho(T)$ shows a resistivity minimum at $T_{\rm min}$. $T_{\rm min}$ is sample dependent, varying from larger than 300 K to 170 K, with an average of 210 K. It is unclear whether $T_{\rm min}$ comes from disorder or other mechanisms, such as charge gap formation. With decreasing temperature, an abrupt resistivity increase with a bump feature occurs below ∼100 K. No hysteresis is observed between zero field cooling (ZFC) and warming $\rho(T)$ data. The inset shows the temperature derivative of the electrical resistivity $d\rho/dT$ obtained at $H = 0$ and 9 T. The parent 10-3-8 compound shows two kinks at $T_1 = 103$ K and $T_2 = 95$ K in $d\rho/dT$. These features are also observed in underdoped $Ba(Fe_{1-x}Co_x)_2As_2$,[15] where the higher temperature kink is related to the structural phase transition and the lower temperature kink is related to the magnetic phase transition,[16] suggesting that a structural phase transition in the parent 10-3-8 phase may occur at 103 K and a magnetic phase transition may occur at 95 K. No change in the temperature of the anomalies is observed with 9 T applied field. Figure 2(b) shows the temperature dependent susceptibility $\chi(T)$ taken at 4 T. At 300 K, the susceptibility is around 1×10^{-3} emu/mol, similar to that of $BaFe_2As_2$. Unlike the linear temperature dependence observed in $BaFe_2As_2$ (Refs. 17 and 18) at high temperatures, from 300 to 100 K, the susceptibility is only weakly temperature dependent with a minimum around 200 K. As temperature decreases, a drop in susceptibility is observed at ∼100 K, which is shown in the inset of Fig. 2(b). This susceptibility drop is consistent with the resistivity measurement and supports the existence of a magnetic/structural phase transition despite the highly two-dimensional crystal structure. Below 80 K, a Curie tail is observed, which may be caused by magnetic impurities. This paramagnetic contribution combines with the intrinsic magnetism and may lead to the weakly temperature dependent susceptibility from 200 to 300 K. Figure 2(c) shows the temperature dependent specific heat data. A clear specific heat anomaly is observed around 100 K, which is consistent with both $\rho(T)$ and $\chi(T)$ data. Below 5 K, assuming there are no magnetic excitations, C_p/T obeys the relation of $C_p/T = \gamma + \beta T^2$, with an electronic specific heat coefficient $\gamma = 4.8$ mJ/mol Fe_2 K^2 and $\beta = 0.95$ mJ/mol Fe_2 K^3, corresponding to a Debye temperature of 256 K.

TABLE I. The nominal Ca:La:Fe:Pt:As ratio in the crystal growth. WDS measured doping level x.

$(Ca_{1-x}La_x)_{10}(Pt_3As_8)(Fe_2As_2)_5$							
Nominal Ca	3.5	3.45	3.4	3.35	3.3	4.1	4.2
Nominal La	0	0.05	0.1	0.15	0.2	0.4	0.8
Nominal Fe	2	2	2	2	2	2	2
Nominal Pt	0.4	0.4	0.4	0.4	0.4	0.4	0.4
Nominal As	5.5	5.5	5.5	5.5	5.5	6.5	7
x	0	0.021	0.043	0.065	0.093	0.145	0.182

The evolution of the $(Ca_{1-x}La_x)_{10}(Pt_3As_8)(Fe_2As_2)_5$ series with doping is presented in Fig. 3. Figure 3(a) shows the temperature dependent Hall coefficient for the $x = 0$ and $x = 0.145$ compounds. The negative Hall coefficient indicates the dominant role of electrons. A dramatic slope change of $\log_{10}|R_H|$, indicating a gap opening related to the structural/magnetic phase transition, is observed in the parent compound, but not in the $x = 0.145$ compound. Within the single band model, the carrier concentration is determined from $n = -1/eR_H$, which leads to $n^{x=0}_{300\,\rm K} = 8.7\times10^{21}$ cm^{-3} and $n^{x=0.145}_{300\,\rm K} = 1.06\times10^{22}$ cm^{-3}. Using the unit cell volume $V = 788.1$ Å^3,[5] the estimated extra carrier concentration due to the La doping is $(n^{x=0.145}_{300\,\rm K} - n^{x=0}_{300\,\rm K})\times V = 1.5$/unit cell. This number is consistent with the WDS measurement assuming one La atom adds one electron. Figure 3(b) shows the temperature dependent normalized resistivity $R/R_{300\,\rm K}$. The high temperature resistive bump is suppressed to 87 K in the

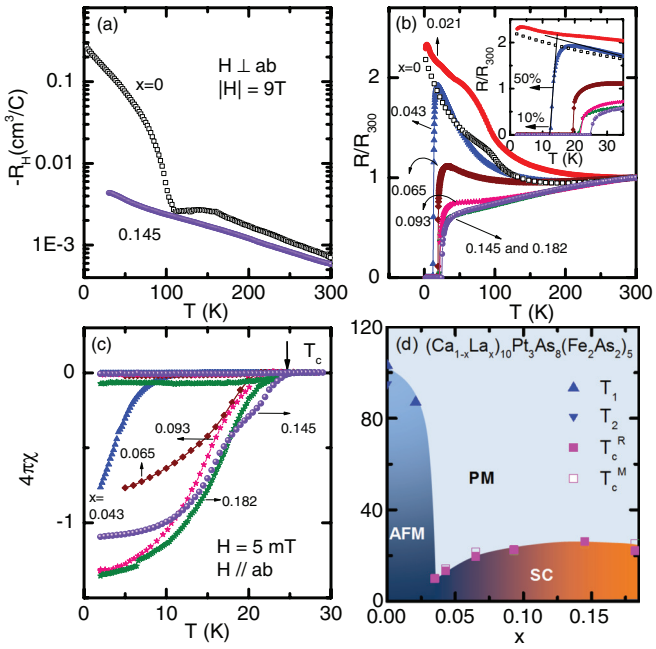

FIG. 3. (Color online) The evolution of the $(Ca_{1-x}La_x)_{10}(Pt_3As_8)(Fe_2As_2)_5$ series with doping. (a) Negative Hall coefficient $-R_H(T)$ for $x = 0$ and 0.145 compositions. (b) The temperature dependent $R/R_{300\,K}$. Inset: The amplified $R/R_{300\,K}$. (c) The ZFC and FC $4\pi\chi$ taken at 5 mT with H along the ab plane. (d) The temperature-concentration phase diagram. It is unclear if there is a coexistence region of antiferromagnetism and superconductivity.

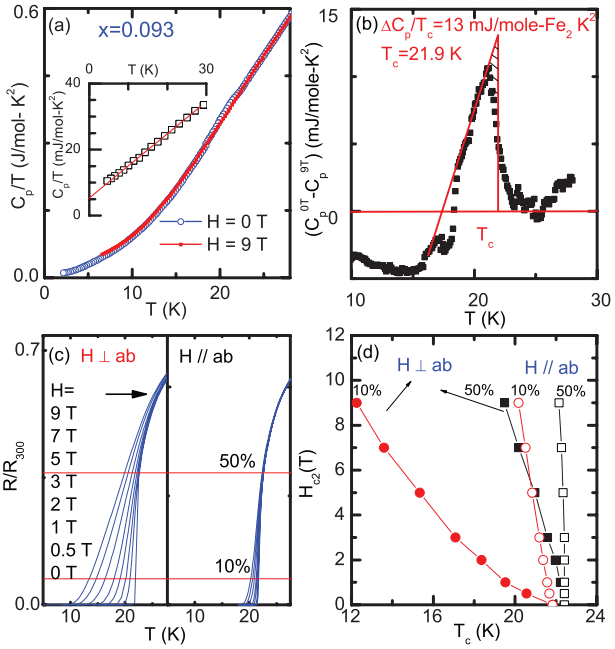

FIG. 4. (Color online) Physical properties of the superconducting state in the $x = 0.093$ 10-3-8 compound. (a) C_p/T vs T in $H = 0$ T (open squares) and 9 T (solid line). Inset: C_p/T vs T^2 in 0 T. (b) $(C_p^{0\,T} - C_p^{9\,T})/T$ vs T. T_c is inferred using the equal entropy construction shown in (c) $R/R_{300\,K}$ taken at $H = 0, 0.5, 1, 2, 3, 5, 7$, and 9 T with H along and perpendicular to the ab plane. (d) H_{c2} vs T obtained with the 10% and 50% criteria from the resistivity data in (c). The units of heat capacity presented are normalized to per mole Fe_2.

$x = 0.021$ compound. No resistive bump is detected when $x \geqslant 0.043$. Comparing with the Pt doped 10-3-8 series,[5,8] this implies that no structural phase transition occurs. For the samples with $x \leqslant 0.093$, the normal state resistance shows a resistivity minimum at T_{min}. Although T_{min} is sample dependent, its average value decreases with increasing doping and disappears at $x = 0.145$. From the pieces we measured, the average T_{min} is 210 ± 30 K for $x = 0$, 200 ± 15 K for $x = 0.021$, 180 ± 30 K for $x = 0.043$, 130 ± 40 K for $x = 0.065$, and 70 ± 5 K for $x = 0.093$. Superconductivity occurs when $x \geqslant 0.043$. Using the 50% criterion shown in the inset of Fig. 3(b), T_c first appears at 13.3 K in the $x = 0.043$ sample, rises to 26.1 K in the $x = 0.145$ sample, and then decreases to 22.1 K in the $x = 0.182$ sample. Figure 3(c) presents ZFC and FC susceptibility data taken at 5 mT with $H \parallel ab$. The criterion to infer T_c is shown in the figure. Although the transitions are broader compared to $Ba(Fe_{1-x}Co_x)_2As_2$ single crystals, the large shielding fraction is comparable to the 122 series, which indicates bulk superconductivity. A small Meissner fraction is a common feature in Fe-pnictide superconductors and is attributed to flux pinning. The temperature-composition phase diagram, constructed from the above physical properties, is shown in Fig. 3(d). With La doping, the structural/magnetic phase transitions are suppressed and superconductivity occurs, with a maximum T_c around 26.1 K at $x = 0.145$. Due to difficulty in controlling the doping level precisely around $x = 0.03$, it is not yet clear whether there is a coexistence region of AFM and superconductivity, nor is it clear how T_2 evolves with doping. Further work is necessary to resolve these issues.

To study the superconducting state of the La doped 10-3-8 superconductors in detail, a representative sample with $x = 0.093$ was chosen. Figure 4(a) shows the specific heat measured at $H = 0$ and 9 T with $H \perp ab$. A specific heat jump can be observed, confirming bulk superconductivity. The inset shows C_p/T vs T^2 taken at $H = 0$ T. The inferred residual γ is 5.8 mJ/mol Fe_2 K^2 and the Debye temperature is 257 K. Figure 4(b) shows a plot of $(C_p^{0\,T} - C_p^{9\,T})/T$ vs T. Using an equal entropy construction shown in Fig. 4(b), the resulting $\Delta C_p/T_c$ is 13 mJ/mol Fe_2 K^2 and T_c is 21.9 K. These values fall onto the Budko-Ni-Canfield (BNC) log-log plot reasonably well,[19–21] adding one more example to the BNC scaling, which reveals $\Delta C_p/T_c$ is proportional to T_c^2 for a large number of 122, 111, and 1111 based superconductors. The calculated γ_n (Ref. 22) is 16 ± 2 mJ/mol Fe_2 K^2, leading to $\Delta C_p/T_c\gamma_n \sim 0.8$. Figure 4(c) shows the suppression of T_c under an applied magnetic field, in which the resistive transition becomes much broader, indicating strong thermal fluctuations of vortices in this compound. Since T_c is suppressed by less than 0.1 K using the 90% criterion when 9 T is applied along ab plane, only the 50% and 10% criteria are employed to infer T_c under field. The derived upper critical field $H_{c2}(T)$ is summarized in Fig. 4(d). The orbital limiting $H_{c2}(0)$ can be calculated via the WHH equation $-0.69T_c dH_{c2}/dT|_{T_c}$. Using the 50% criterion, the estimated $H_{c2}^{\parallel ab}(0) \sim 400$ T and $H_{c2}^{\perp ab}(0) \sim 60$ T; using the 10% criterion, the estimated $H_{c2}^{\parallel ab}(0) \sim 70$ T and $H_{c2}^{\perp ab}(0) \sim 10$T. $H_{c2}^{\parallel ab}(0)$ obtained from

50% criterion is almost four times of that in $SmFeAsO_{0.8}F_{0.2}$ with a T_c of 40 K, implying a very large gap formation. Although the $H_{c2}^{\perp ab}$ curve inferred from the 50% criterion shows roughly linear behavior, the $H_{c2}^{\perp ab}$ curve inferred from the 10% criterion shows upward curvature, which is common in cuprate and multigap 1111 superconductors.[23–25]

In conclusion, we have characterized superconducting $(Ca_{1-x}La_x)_{10}(Pt_3As_8)(Fe_2As_2)_5$ ($x = 0$–0.182) single crystals. With La doping, the structural/magnetic phase transitions around 100 K in the pure 10-3-8 compound are suppressed. Bulk superconductivity occurs at 13.3 K at 4.4% doping, rises to 26.1 K at 14.5% doping, and then decreases to 22.1 K at 18.2% doping.

Work at Los Alamos was performed under the auspices of the US Department of Energy, Office of Science, Division of Materials Science and Engineering. Work at Princeton University was supported by the AFOSR MURI on superconductivity. Work at Ames Laboratory (W.E.S., M.A.T., R.P.) was supported by the US Department of Energy, Office of Basic Energy Science, Division of Materials Sciences and Engineering. Ames Laboratory is operated for the US Department of Energy by Iowa State University under Contract No. DE-AC02-07CH11358. N.N. acknowledges support from a Marie Curie Fellowship at Los Alamos National Laboratory. The authors thank Eunsung Park, Xin Lu, and Ryan Baumbach for useful discussions.

[1] Y. Kamihara, T. Watanabe, M. Hirano, and H. Hosono, J. Am. Chem. Soc. **130**, 3296 (2008).

[2] M. Rotter, M. Tegel, and D. Johrendt, Phys. Rev. Lett. **101**, 107006 (2008).

[3] X. C. Wang, Q. Q. Liu, Y. X. Lv, W. B. Gao, L. X. Yang, R. C. Yu, F. Y. Li, and C. Q. Jin, Solid State Commun. **148**, 538 (2008).

[4] X. Zhu, F. Han, G. Mu, P. Cheng, B. Shen, B. Zeng, and H.-H. Wen, Phys. Rev. B **79**, 220512(R) (2009).

[5] N. Ni, J. M. Allred, B. C. Chan, and R. J. Cava, Proc. Natl. Acad. Sci. USA **108**, E1019 (2011).

[6] S. Kakiya, K. Kudo, Y. Nishikubo, K. Oku, E. Nishibori, H. Sawa, T. Yamamoto, T. Nozaka, and M. Nohara, J. Phys. Soc. Jpn. **80**, 093704 (2011).

[7] C. Lohnert, T. Sturzer, M. Tegel, R. Frankovsky, G. Friederichs, and D. Johrendt, Angew. Chem. Int. Ed. **50**, 9195 (2011).

[8] K. Cho, M. A. Tanatar, H. Kim, W. E. Straszheim, N. Ni, R. J. Cava, and R. Prozorov, Phys. Rev. B **85**, 020504(R) (2012).

[9] Z. J. Xiang, X. G. Luo, J. J. Ying, X. F. Wang, Y. J. Yan, A. F. Wang, P. Cheng, G. J. Ye, and X. H. Chen, Phys. Rev. B **85**, 224527 (2012).

[10] T. Zhou, G. Koutroulakis, J. Lodico, Ni Ni, J. D. Thompson, S. E. Brown, and R. J. Cava, arXiv:1212.3901.

[11] T. Stürzer, G. Derondeau, and D. Johrendt, Phys. Rev. B **86**, 060516(R) (2012).

[12] T. J. B. Holland and S. A. T. Redfern, Mineral. Mag. **61**, 65 (1997).

[13] M. A. Tanatar, N. Ni, A. Thaler, S. L. Budko, P. C. Canfield, and R. Prozorov, Phys. Rev. B **82**, 134528 (2010).

[14] N. Spyrison, M. A. Tanatar, K. Cho, Y. Song, P. Dai, C. Zhang, and R. Prozorov, Phys. Rev. B **86**, 144528 (2012).

[15] N. Ni, A. Thaler, J. Q. Yan, A. Kracher, E. Colombier, S. L. Budko, P. C. Canfield, and S. T. Hannahs, Phys. Rev. B **82**, 024519 (2010).

[16] D. K. Pratt, W. Tian, A. Kreyssig, J. L. Zarestky, S. Nandi, N. Ni, S. L. Budko, P. C. Canfield, A. I. Goldman, and R. J. McQueeney, Phys. Rev. Lett. **103**, 087001 (2009).

[17] G. M. Zhang, Y. H. Su, Z. Y. Lu, Z. Y. Weng, D. H. Lee, and T. Xiang, Europhys. Lett. **86**, 37006 (2009).

[18] X. F. Wang, T. Wu, G. Wu, H. Chen, Y. L. Xie, J. J. Ying, Y. J. Yan, R. H. Liu, and X. H. Chen, Phys. Rev. Lett. **102**, 117005 (2009).

[19] S. L. Budko, N. Ni, and P. C. Canfield, Phys. Rev. B **79**, 220516(R) (2009).

[20] G. R. Stewart, Rev. Mod. Phys. **83**, 1589 (2011).

[21] J. S. Kim, B. D. Faeth, and G. R. Stewart, Phys. Rev. B **86**, 054509 (2012).

[22] We assume the phonon contribution of the $x = 0$ and $x = 0.145$ samples obey the law of corresponding states. Then the electronic specific heat of the $x = 0.145$ sample is obtained using $C_e^{x=0.145} = C_p^{x=0.145} - AC_{\text{phonon}}^{x=0}$, where $C_{\text{phonon}}^{x=0}$ is obtained by subtracting the electronic part from $C_p^{x=0}$. A and $\gamma_n^{x=0.145}$ are thus determined by enforcing $\int_0^{T_C} \gamma_n^{x=0.145} dT = \int_0^{T_C} C_e^{x=0.145}/TdT$.

[23] H.-S. Lee, M. Bartkowiak, J.-H. Park, J.-Y. Lee, J.-Y. Kim, N.-H. Sung, B. K. Cho, C.-U. Jung, J. S. Kim, and H.-J. Lee, Phys. Rev. B **80**, 144512 (2009).

[24] A. P. Mackenzie, S. R. Julian, G. G. Lonzarich, A. Carrington, S. D. Hughes, R. S. Liu, and D. C. Sinclair, Phys. Rev. Lett. **71**, 1238 (1993).

[25] F. Hunte, J. Jaroszynski, A. Gurevich, D. C. Larbalestier, R. Jin, A. S. Sefat, M. A. McGuire, B. C. Sales, D. K. Christen, and D. Mandrus, Nature (London) **453**, 903 (2008).